Effect of surface ionic screening on the polarization reversal scenario in ferroelectric thin films: Crossover from ferroionic to antiferroionic states

Anna N. Morozovska,[1,2,*] Eugene A. Eliseev,[3] Anatolii I. Kurchak,[4] Nicholas V. Morozovsky,[1] Rama K. Vasudevan,[5] Maksym V. Strikha,[4,6] and Sergei V. Kalinin[5,*]

[1]*Institute of Physics, National Academy of Sciences of Ukraine, pr. Nauky 46, 03028 Kyiv, Ukraine*

[2]*Bogolyubov Institute for Theoretical Physics, National Academy of Sciences of Ukraine, 14-b Metrolohichna str. 03680 Kyiv, Ukraine*

[3]*Institute for Problems of Materials Science, National Academy of Sciences of Ukraine, Krjijanovskogo 3, 03142 Kyiv, Ukraine*

[4]*V.Lashkariov Institute of Semiconductor Physics, National Academy of Sciences of Ukraine, pr. Nauky 41, 03028 Kyiv, Ukraine*

[5]*The Center for Nanophase Materials Sciences, Oak Ridge National Laboratory, Oak Ridge, Tennessee 37831, USA*

[6]*Taras Shevchenko Kyiv National University, Radiophysical Faculty pr. Akademika Hlushkova 4g, 03022 Kyiv, Ukraine*

(Received 31 October 2017; published 8 December 2017)

Nonlinear electrostatic interaction between the surface ions of electrochemical nature and ferroelectric dipoles gives rise to the coupled ferroionic states in nanoscale ferroelectrics. Here, we investigate the role of the surface ion formation energy on the polarization states and its reversal mechanisms, domain structure, and corresponding phase diagrams of ferroelectric thin films. Using 3D finite element modeling, we analyze the distribution and hysteresis loops of ferroelectric polarization and ionic charge, and the dynamics of the domain states. These calculations performed over large parameter space delineate the regions of single- and polydomain ferroelectric, ferroionic, antiferroionic, and nonferroelectric states as a function of surface ion formation energy, film thickness, applied voltage, and temperature. We further map the analytical theory for 1D systems onto an effective Landau-Ginzburg free energy and establish the correspondence between the 3D numerical and 1D analytical results. This approach allows us to perform an overview of the ferroionic system phase diagrams and explore the specifics of polarization reversal and domain evolution phenomena.

DOI: 10.1103/PhysRevB.96.245405

I. INTRODUCTION

Ferroelectric phase stability requires effective screening of the polarization bound charge at surfaces and interfaces with nonzero normal components of polarization [1–3]. Traditionally, the theoretical analysis of bulk ferroelectric states assumes either complete screening of polarization by conducting electrodes or considers the emergence of the multidomain states as a pathway to minimize depolarization energy [1–3]. The rapid growth of thin-film applications of ferroelectrics in the 90's necessitated the analysis of the microscopic mechanisms active at ferroelectric interfaces, preponderantly effects stemming from nonzero spatial separation between polarization and screening charges [4–8]. These effects are often introduced via the dead layer [2] or physical gap [9] concepts, postulating the presence of a thin nonferroelectric layer or a gap separating ferroelectric and an electrode. The approach has been shown to agree with *ab initio* calculations [10,11]. Because of the long-range nature of depolarization effects, the incomplete surface screening of ferroelectric polarization leads to pronounced finite size effects [12] and nontrivial domain structure dynamics [1] in the presence of thin dead layers and gaps. These in turn causes unusual phenomena near the electrically opened surfaces such as correlated polarization switching, formation of flux-closure domains in multiaxial ferroelectrics [13–16], and domain wall broadening in uniaxial [17,18] and multiaxial ferroelectrics [15,16]. Further examples of these behaviors include the crossover between different screening regimes in ferroelectric films [19,20] and *p-n* junctions induced in 2D semiconductors [21] separated by the ultrathin gap from the moving domain wall or surface junctions.

However, the dead layer approximation completely ignores many important details of the screening process thermodynamics. In particular, the stabilization of a ferroelectric state in ultrathin perovskite films can take place due to the chemical switching (see, e.g., Refs. [22–24]), and the screening via ionic adsorption is intrinsically coupled to the thermodynamic of surface electrochemical processes. This coupling results in nontrivial effects on ferroelectric phase stability and phase diagrams [25,26]. Similar effects are expected for screening by electrodes with finite density of states [27]. However, the surface states of materials in contact with the atmosphere are usually poorly defined due to the presence of mobile electrochemically active and physically sorbable components in an ambient environment [28,29]. The effect of oxygen and hydrogen adsorption on the work function, reversible polarization value, dipole moment of the unit cell, and free energy of the semiconductor ferroelectrics has been investigated experimentally and theoretically [30–33], albeit the total volume of research in this area is extremely small. Consequently, no comprehensive or general approaches have been developed.

The early theoretical analyses, though studied the properties of ferroelectric materials in details, typically, ignored the nonlinear tunable characteristics of surface screening charges [30–33]. A complementary thermodynamic approach was developed by Stephenson and Highland (SH) [25,26], who consider an ultrathin film in equilibrium with a chemical environment that supplies ionic species (positive and negative) to compensate its polarization bound charge at the surface.

Recently, we modified the SH approach allowing for the presence of a gap between the ferroelectric surface covered

*Corresponding authors: anna.n.morozovska@gmail.com; sergei2@ornl.gov

by ions and the SPM tip [34–37], and developed an analytic description for the thermodynamics and kinetics of these systems. The analysis [34–36] leads to the elucidation of the ferroionic states, which are the result of nonlinear electrostatic interactions between the surface ions, with the charge density obeying the Langmuir adsorption isotherm, and with single-domain ferroelectric polarization. The properties of ferroionic states were described by a system of coupled equations.

Here, we study the stability of ferroionic states with respect to the domain structure formation and polarization reversal scenarios in thin ferroelectric films covered by ions. Our results, presented below, reveal unusual dependencies of the film polar state and domain structure properties on the ion formation energies and their difference, and an even more unexpected dependence on the applied voltage. We predict electric field-induced phase transitions into ferroionic and antiferroionic states in thin films covered with ion layers of electrochemically active nature.

The manuscript is structured as follows. The basic equations with boundary conditions are given in Sec. II. The numerical results presented in Sec. III demonstrate the effect of surface ion formation energy on stable polarization states, evolution of domain structure, and surface charge during polarization reversal. To get insight into the numerical results, in Sec. IV, we present a simplified analytical modeling of the ferroionic system behavior based on the free energy with renormalized coefficients. Distinctive features of polarization reversal in thin ferroelectric films covered by ions are discussed in Sec. V. The electrostatic problem and a derivation of the free energy with renormalized coefficients are given in Appendixes A and B, respectively. The parameters used in the calculations and auxiliary figures are listed in Ref. [38].

II. BASIC EQUATIONS WITH BOUNDARY CONDITIONS

Here, we consider a system consisting of an electron conducting bottom electrode, a ferroelectric (FE) film, and a layer of surface ions with charge density $\sigma(\varphi)$. An ultrathin gap separates the film surface and the top electrode (either an ion conductive planar electrode or a flatted apex of an SPM tip) and provides direct ion exchange with ambient media, as shown in Fig. 1(a). A mathematical statement of the problem is listed in Refs. [35,36] as well as in Appendix A.

We account for the presence of an ultrathin dielectric gap between the probe tip and the ferroelectric surface. At that, the linear equation of state $\mathbf{D} = \varepsilon_0\varepsilon_d\mathbf{E}$ relates the electrical displacement $\mathbf{D}$ and electric field $\mathbf{E}$ in the gap [ε_0 is a universal dielectric constant and $\varepsilon_d \sim 1$ is the relative permittivity of the physical gap media (vacuum, air or inert gas environment)]. A wide band-gap ferroelectric film can be considered dielectric. A quasistatic electric field inside the ferroelectric film φ_f satisfies the electrostatic equations for each of the media (gap and ferroelectric film). The boundary conditions (**BCs**) for the system are the equivalence of the electric potential to the applied voltage U at the top electrode (or SPM tip apex modeled by the flat region $z = -\lambda$) and the equivalence of the normal component of electric displacements to the ionic surface charge density $\sigma[\varphi(\vec{r})]$ at $z = 0$, the continuity of the electric potential and normal component of displacements $D_3 = \varepsilon_0 E_3 + P_3$ and $D_3 = \varepsilon_0\varepsilon_d E_3$ at gap

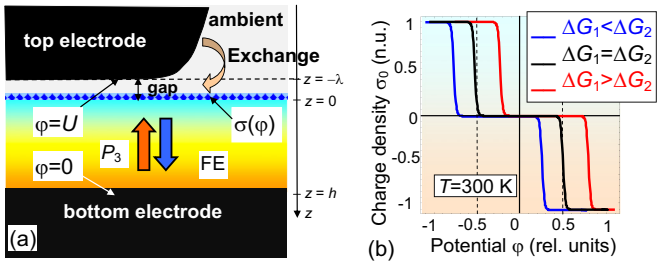

FIG. 1. (a) Layout of the considered system, consisting of an electron conducting bottom electrode, a ferroelectric (FE) film, a surface ions layer with charge density $\sigma(\varphi)$, an ultrathin gap separating film surface, and the top electrode providing direct ion exchange with ambient media (from bottom to the top). (b) Schematic dependence of the equilibrium surface charge density σ_0 vs acting potential φ for $\Delta G_1^{00} < \Delta G_2^{00}$ (blue curve), $\Delta G_1^{00} = \Delta G_2^{00}$ (black curve), and $\Delta G_1^{00} > \Delta G_2^{00}$ (red curve) (adapted from Ref. [35]).

- ferroelectric interface $z = 0$, and zero potential at the bottom conducting electrode $z = h$ [see Fig. 1(a)].

The polarization components of uniaxial ferroelectric film depend on the inner field $\boldsymbol{E}$ as $P_1 = \varepsilon_0(\varepsilon_{11}^f - 1)E_1$, $P_2 = \varepsilon_0(\varepsilon_{11}^f - 1)E_2$ and $P_3(\mathbf{r},E_3) = P_3^f(\mathbf{r},E_3) + \varepsilon_0(\varepsilon_{33}^b - 1)E_3$, where the relative background permittivity $\varepsilon_{33}^b \leqslant 10$ [39]. The relative dielectric permittivity ε_{33}^f is connected with the ferroelectric polarization P_3 via the soft mode. The evolution and spatial distribution of the ferroelectric polarization P_3^f (further abbreviated as P_3) is given by the time-dependent LGD equation

$$\Gamma\frac{\partial P_3}{\partial t} + \alpha P_3 + \beta P_3^3 + \gamma P_3^5 - g\frac{\partial^2 P_3}{\partial z^2} = E_3, \qquad (1)$$

In Eq. (1), the kinetic coefficient Γ is defined by phonon relaxation; $\alpha = \alpha_T(T_C - T)$, β, and $\gamma \geqslant 0$ are the coefficients of LGD potential $F(P_i,X_{ij},\sigma)$ expansion on the higher polarization powers [40]; T is the absolute temperature, and T_C is Curie temperature. The BCs for polarization at the film surfaces $z = 0$ and $z = h$ are of the third kind, $(P_3 \mp \Lambda_{\mp}\frac{\partial P_3}{\partial z})|_{z=0,h} = 0$, and include the extrapolation lengths $\Lambda_{\pm}$ [41,42].

The equation for the surface charge is analogous to the Langmuir adsorption isotherm used in interfacial electrochemistry for adsorption onto a conducting electrode exposed to ions in a solution [43]. To describe the dynamics of surface ions, we use a linear relaxation model for their charge density, $\tau\frac{\partial\sigma}{\partial t} + \sigma = \sigma_0[\varphi]$, where the dependence of equilibrium charge density $\sigma_0[\varphi]$ on the electric potential φ is controlled by the concentration of surface ions $\theta_i(\varphi)$ at the interface $z = 0$ in a self-consistent manner [25,26]:

$$\sigma_0[\varphi] = \sum_{i=1}^{2}\frac{eZ_i\theta_i(\varphi)}{A_i} \equiv \sum_{i=1}^{2}\frac{eZ_i}{A_i}\left[1 + \left(\frac{p_{\text{atm}}}{p_{\text{exc}}}\right)^{1/n_i}\exp\left(\frac{\Delta G_i^{00} + eZ_i\varphi}{k_BT}\right)\right]^{-1}, \qquad (2)$$

where e is an elementary charge, Z_i is the ionization degree of the surface ions/electrons, $1/A_i$ are the saturation densities of the surface ions, at that, the subscript i designates the summation on positive ($i = 1$) and negative ($i = 2$) charges, respectively, p_{exc} is the partial pressure of ambient gas relative to atmospheric pressure p_{atm}, and n_i is the number of surface ions created per gas molecule. Two surface charge species exist since the gas molecule had been electroneutral before its electrochemical decomposition started.

Positive parameters ΔG_1^{00} and ΔG_2^{00} are the free energies of the surface defect formation at $p_{exc} = 1$ bar and zero applied voltage $U = 0$. The energies ΔG_i^{00} are responsible for the formation of different surface ionic states (ions, vacancies, etc). Specifically, the values ΔG_i^{00} are poorly known and typically vary in the range ~(0–1) eV [25], and the difference $\Delta G_1^{00} - \Delta G_2^{00}$ can play a crucial role in the overall behavior of a ferroelectric film covered by ions (as it will be shown below). Thus experiments and *ab initio* calculations of ΔG_i^{00} values are urgently required for many practically important cases.

A schematic steplike dependence of the surface charge density σ_0 on the potential φ is shown in Fig. 1(b). The surface charge is almost zero in the region $\varphi_1 < \varphi < \varphi_2$, and then it abruptly increases for potential values $\varphi_i \approx -\Delta G_i^{00}/(eZ_i)$ ($i = 1, 2$). The abrupt steplike dependence is left-shifted with respect to $\varphi = 0$ for $\Delta G_1^{00} < \Delta G_2^{00}$ (blue curve), almost antisymmetric for $\Delta G_1^{00} \approx \Delta G_2^{00}$ (black curve) and right-shifted for $\Delta G_1^{00} > \Delta G_2^{00}$ (red curve). For equal $\Delta G_1^{00} = \Delta G_2^{00} \equiv \Delta G$, the Langmuir isotherm is the even function of ΔG, namely $\sigma_0(\varphi, \Delta G) \equiv \sigma_0(\varphi, -\Delta G)$, provided that other parameters correspond to the charge neutrality at zero potential. Notably, the developed solutions are insensitive to the specific details of the charge compensation process [44], and are sensitive only to the thermodynamic parameters of the corresponding reactions [45].

III. EFFECT OF SURFACE IONS FORMATION ENERGY ON POLARIZATION REVERSAL AND DOMAIN STRUCTURE. FEM RESULTS

Using 3D finite element modeling (FEM), we studied the polarization states in the ferroionic system. Following the terminology introduced in Refs. [34–36], we classified the possible polar state in the ferroionic system based on the free energy minima and hysteresis loop shape. A general property of the ferroelectric film covered with ions is that it can be in the single-domain (SD) or polydomain (PD) ferroelectric (FE), ferroionic (FI), antiferroionic (AFI), and ionic nonferroelectric (NFE) equilibrium states depending on the applied voltage U,

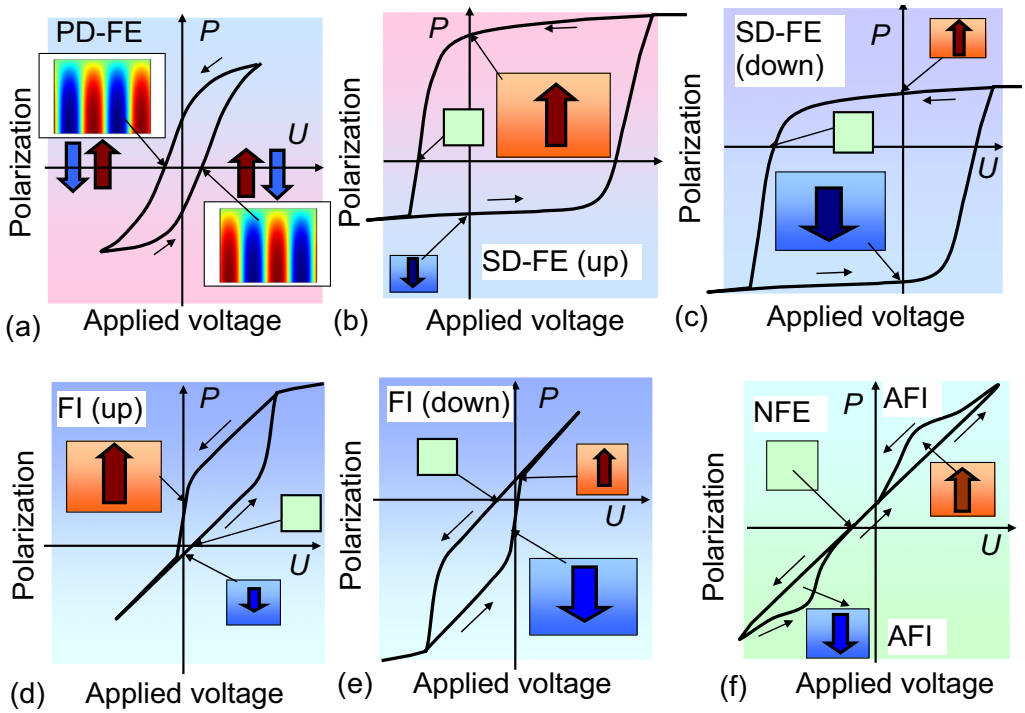

FIG. 2. (a)–(c) Polar states classification in the ferroionic system based on the polarization distribution and hysteresis loop form. The x axis is the applied voltage U, the y axis is the average polarization P. Characteristic hysteresis loops for a polydomain ferroelectric (PD-FE) state (a), positive (b) and negative (c) single-domain ferroelectric (SD-FE) states with dominant "upward" and "downward" polarizations, positive (d) and negative (e) ferroionic (FI) states with almost "upward" and "downward" polarizations, and (f) mixed antiferroionic (AFI) and ionic nonferroelectric (NFE) states are shown. Polarization distribution corresponding to definite points at the hysteresis loop is shown by insets in the form of colored squares with upward or downward oriented arrows for a single-domain state, two upward and downward oriented arrows for a polydomain state (accomplished by the snapshot of the stripe domains broadening near the surface), and an empty light-green square for a zero homogeneous polarization. The smooth gradient filling (reddish or bluish) of the insets with arrows indicates a slight decrease of the polarization value near the top surface $z = 0$ that is covered by ions and separated by an ultrathin gap from the tip electrode. The slight decrease is induced by depolarization field.

temperature T, film thickness h, and ion formation energies ΔG_i^{00} (see Fig. 2).

The **FE** state is defined as the state with robust ferroelectric hysteresis between at least two (or more) absolutely stable ferroelectric polarizations, which have "positive" or "negative" projections with respect to the film surface normal [see Figs. 2(a)–2(c)]. Due to the nonlinear voltage dependence of the surface ion charge density [see Eq. (2)], the polarization screening by surface ions results in one or more unstable positive or negative polarization states. FE states exist at film thickness above the critical value, $h \geqslant h_{\rm cr}(T)$, at fixed temperature $T < T_C$. Usually, the value $h_{\rm cr}(T)$ depends on the screening conditions [1,15,16]. Due to the presence of the gap between the film surface and the tip electrode, FE states can be polydomain (**PD-FE**) with a rather thin and tilted hysteresis loop at small amplitudes of applied voltage [see Figs. 2(a)]. Also FE states can be almost single-domain (**SD-FE**) with symmetric, dominantly positive or negative polarizations, and correspond to a wide squarelike hysteresis loop at higher voltage amplitudes [see Figs. 2(b) and 2(c)]. Noteworthy, SD-FE states can be more stable than the PD-FE ones for $\Delta G_1^{00} \neq \Delta G_2^{00}$, because positive and negative orientations of polarization are energetically equivalent only at zero applied voltage $U = 0$. The physical origin of SD-FE states voltage asymmetry is the electric field of electrochemical nature, $E_{\rm eff} \sim (\Delta G_1^{00} - \Delta G_2^{00})/h$, produced by surface ions with the charge density $\sigma(U)$. The field $E_{\rm eff}$ was introduced earlier [34–36] and its analytical form will be discussed in the next section. When $E_{\rm eff}$ exceeds a certain critical value, the SD-FE state becomes absolutely stable and the PD-FE state becomes metastable.

The **FI** state appears with increase of $E_{\rm eff}$ as supported by the voltage bistability of ionic states and its boundary with SD-FE stable is conditional (resembling relative definition of ferroelectric and pyroelectric). The FI state is characterized by a strongly asymmetric, horizontally shifted or vertically imprinted hysteresis loop between two polarization states (one is stable and another is metastable) with the same polarization direction [Figs. 2(d) and 2(e)]. In contrast to the PD-FE state, the polarization direction practically does not change for all points on the hysteresis loop in the FI states, i.e., it remains positive [see the loop with almost positive polarization and the very small region with negative polarization in Fig. 2(d)] or negative [see the loop in Fig. 2(e)]. FI states appear because one of the polarization orientations loses its stability when the film thickness h becomes less than the critical value $h_{\rm cr}(T)$, and can exist for significantly different values of ΔG_i^{00} (e.g., for $|\Delta G_1^{00} - \Delta G_2^{00}| \geqslant 0.2\,{\rm eV}$) even in ultrathin films ($h \leqslant 2\,{\rm nm}$) at high temperatures [2].

The NFE state follows the FI state when the temperature increases or the film thickness decreases more, well below the critical value $h_{\rm cr}(T)$. The NFE state [shown by a light green squire without arrow in Fig. 1(f)] appears when two metastable polarization orientations [shown in Fig. 1(f) by reddish and bluish squires with upward and downward arrows] disappear under the voltage decrease. The NFE state has no hysteresis properties at $U = 0$ in the thermodynamic limit and reveals an electretlike polarization state $P_3 \sim E_{\rm eff}(\sigma)$ induced by the field $E_{\rm eff}$ [see Fig. 2(f)].

A double hysteresis loop opening that appears at high applied voltages U corresponds to the novel antiferroionic (**AFI**) state. Since the energies of upward and downward polarization orientations gradually reach each other with the temperature increase, the diffuse boundary between AFI and FI states is defined by the electrochemical properties of surface ions, in particular, by the ion formation energies ΔG_i^{00}.

Stable polarization states were calculated numerically in dependence on the surface ion formation energies ΔG_i^{00} at zero applied voltage ($U = 0$); the corresponding diagrams are shown in Figs. [3(a)–3(c)] for 100-nm, 50-nm, and 10-nm PZT films, respectively. Here, the calculations are performed for the relative permittivity of the dielectric gap $\varepsilon_d = 1$, its thickness $\lambda = 0.4\,{\rm nm}$ and saturation area of the surface ions $A_1 = A_2 = 10^{-18}\,{\rm m}^2$. Other parameters are listed in Table SI Ref. [38].

Green circles in the diagrams Figs. 3(a) and 3(b) correspond to the PD-FE state, blue and orange circles are negative and positive SD-FE states, which continuously transform into FI states. Dashed curves correspond to the contours of constant intrinsic electric field $E_{\rm eff}$ induced by ions. Solid curves are drawn by eye. Note that the domain states in the regions between dashed and solid curves [some of the circles are semicolored in Figs. 3(a) and 3(b)] are very sensitive to the initial seeding (random polarization distribution at $t = 0$), and the film in the average (even being poly-domain) can have a nonzero unipolarity degree, i.e., the fraction (sizes and/or number) of domains with negative polarization orientation is not equal to the fraction with positive one.

A comparison of the polarization states diagram of a 100-nm film [Fig. 3(a)] with the one of a 50-nm film [Fig. 3(b)] shows that the region of PD-FE states (green circles between the solid curves) that extends from the diagonal $\Delta G_1^{00} = \Delta G_2^{00}$ becomes much thinner and smaller with decreasing film thickness. For a 50-nm film, the region narrows to the diagonal at $\Delta G_1^{00} = \Delta G_2^{00} \leqslant 0.7\,{\rm eV}$ and only then slightly enlarges at $0.7 < \Delta G_i^{00} \leqslant 1\,{\rm eV}$. The regions of positive and negative SD-FE states, which are induced by the intrinsic field $E_{\rm eff}$, expand with the increase of the difference $|\Delta G_1^{00} - \Delta G_2^{00}|$. Also, the region of the SD-FE state significantly increases with decreasing film thickness h because $E_{\rm eff} \sim (\Delta G_1^{00} - \Delta G_2^{00})/h$. Note that the regions of the FI state are located far from the diagonal at $|\Delta G_1^{00} - \Delta G_2^{00}| \geqslant 0.8\,{\rm eV}$ and slightly expand with increasing h.

The diagram for the thinnest 10-nm film is very different from the ones for 50- and 100-nm films [see Fig. 3(a)]. The FE states are absent for the case, because the 10-nm film is paraelectric at $\sigma = 0$. Light green, blue, and orange circles in the diagram (c) correspond to the electretlike NFE states, and FI states with negative and positive polarizations, respectively. The film is in a paraelectric state along the diagonal, $\Delta G_1^{00} = \Delta G_2^{00}$. A wide almost square region of NFE states corresponds to $\Delta G_i^{00} \geqslant 0.2\,{\rm eV}$. Note that the NFE states in the regions between dashed and solid lines are very sensitive to the mesh details, and the film (being in an NFE state) has a nonzero average polarization [all of the circles are semi-colored in Fig. 3(c)]. Alternatively, NFE states can be metastable (or slowly relaxing one), and their dynamics is difficult to capture via a numerical model. Stable "up" and "down" FI states, which are caused by $E_{\rm eff}$ increase, are located in the two rectangles with rounded edges,

$0 \leqslant \Delta G_i^{00} \leqslant 0.15$ eV. Note that the unusual physical picture shown in Fig. 3(c) corresponds to the stable polarization states at zero voltage $U = 0$.

The voltage dependencies of polarization $P(U)$ and surface charge $\sigma(U)$ were calculated at relatively high amplitudes of applied voltage U ($U_{max} = 20$ V) for a 10-nm PZT film (corresponding applied field is 2 GV/m). Results for $P(U)$ and $\sigma(U)$ are shown in Figs. 4(a) and 4(b), respectively. These graphs indicate that symmetric, slightly or strongly asymmetric, and double hysteresis loops with pronounced coercive voltage (about 10 V) exist at $\Delta G_i^{00} \leqslant 0.5$ eV. It is worth to note that the spontaneous ferroelectric polarization disappears at zero voltage for $\Delta G_i^{00} > 0.2$ eV [as it is shown in Fig. 3(c)].

Comparison of the loops shown in Fig. 4(a) with the points on the diagram Fig. 3(c) corresponding to the same pair of ion formation energies $\{\Delta G_1^{00}, \Delta G_2^{00}\}$ leads to the following conclusions. If the film was in an FI state at $U = 0$, it remains in the state with increasing voltage amplitude, at that, the polarization reversal along the asymmetric hysteresis loop (or symmetric loop with linear sides untypical for electroded ferroelectrics) follows the single-domain scenario. When the

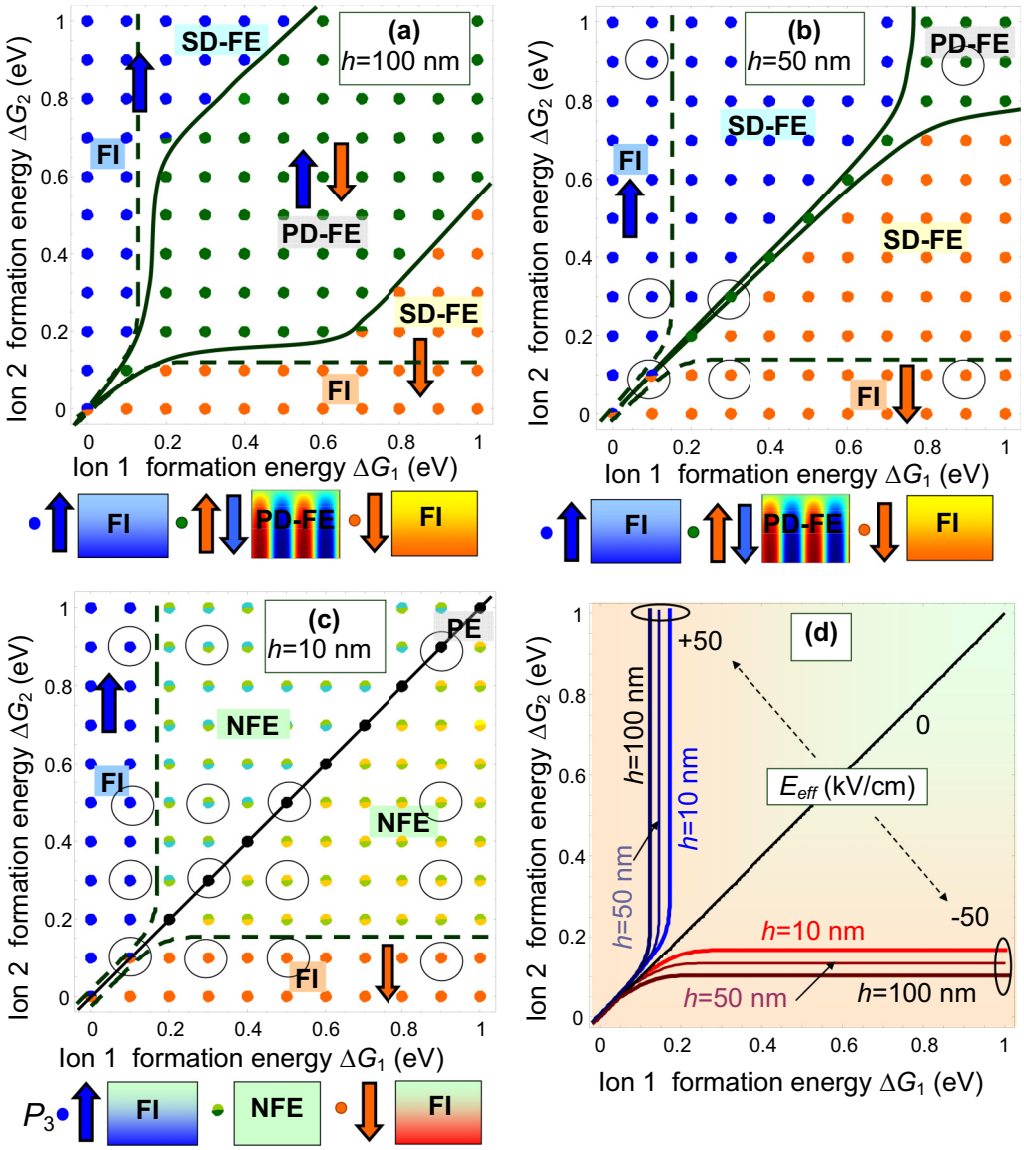

FIG. 3. Polarization states in dependence on the surface ion formation energies ΔG_i^{00} calculated for PZT film thickness $h = 100$ (a), 50 (b), and 10 nm (c). In the diagrams [(a) and (b)], dark green circles correspond to the polydomain ferroelectric state (PD-FE). Single-domain ferroelectric (SD-FE) states with opposite (negative and positive) polarization orientations are represented by blue and orange circles, respectively. SD-FE states continuously transform into ferroionic (FI) states (represented by blue and orange circles). In the diagram (c), black, light yellow-green, blue and orange circles correspond to the paraelectriclike (PE) state, electretlike nonferroelectric (NFE) states, and ferroionic (FI) states with opposite polarization directions, respectively. Solid curves are drawn by eye. (d) Effective intrinsic field $E_0[\Delta G_i^{00}, h]$ (in kV/cm) depending on the surface ion formation energies ΔG_i^{00} calculated for PZT film thickness $h = 10$, 50, and 100 nm (legends at the curves) at $T = 300$ K; other parameters are listed in Table SI in Ref. [38]. Empty rings in the diagrams (b) and (c) indicate the points where the dependencies $P(U)$ are shown in Fig. 4 and S1–S4 in Ref. [38].

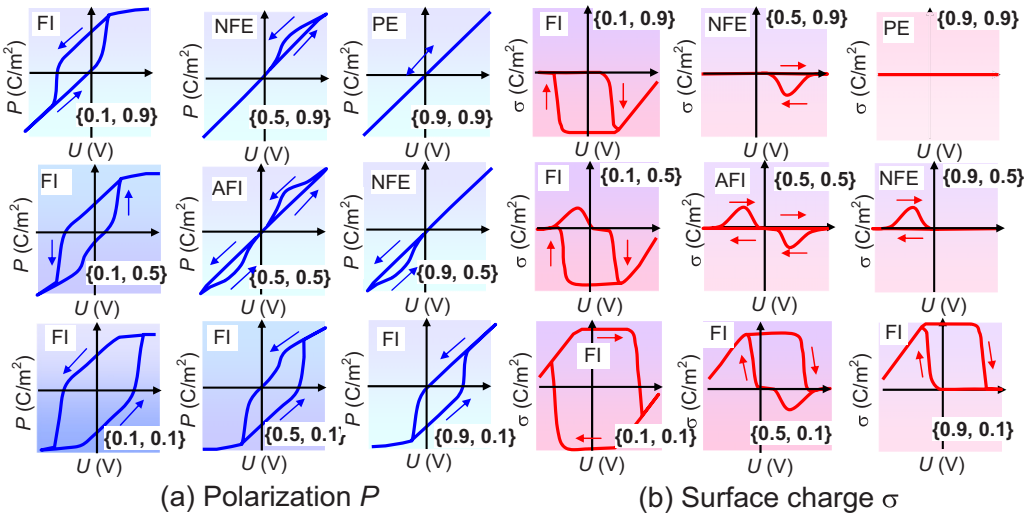

FIG. 4. Dependencies of average polarization $P(U)$ (a) and surface charge $\sigma(U)$ (b) on applied voltage U calculated at fixed values $\{\Delta G_1^{00}, \Delta G_2^{00}\}$ indicated in the labels (in eV) for a 10-nm PZT film. The voltage varies from -20 to $+20$ V. Polarization varies from -0.45 to $+0.45\,\mathrm{C/m^2}$. Surface charge varies from -0.35 to $+0.35\,\mathrm{C/m^2}$. Other parameters are the same as in Fig. 2. Arrows indicate the direction of the loops pass-tracing. Labels "FI", "AFI", "NFE," and "PE" indicate corresponding states.

film is in an NFE state at $U = 0$, it can remain NFE with the voltage increase at the small difference $|\Delta G_1^{00} - \Delta G_2^{00}| \leqslant 0.1$ eV. When the difference $|\Delta G_1^{00} - \Delta G_2^{00}|$ increases and becomes higher than 0.2 eV, the 10-nm film in the NFE state unexpectedly becomes FI with the increasing voltage because asymmetric hysteresis loops with pronounced width and height appear at $U > 10$ V [see the plots with a legend "FI" in Figs. 4(a) and 4(b)]. Hysteresis loops of $P(U)$ and $\sigma(U)$ calculated for more pairs of $\{\Delta G_1^{00}, \Delta G_2^{00}\}$ and $h = 10$ nm are shown in Figs. S1-S2, where the labels "FE, FI, AFI, NFE," and "PE" indicate the corresponding states. Specifically, the FI- and AFI-hysteresis loops of $P(U)$ and $\sigma(U)$ occur with decreasing $|\Delta G_i^{00}|$ (see the right bottom corner in Figs. S1-S2). One can see from Figs. 4, S1, and S2 that pronounced FI hysteresis loops of $P(U)$ and $\sigma(U)$ with high enough coercive voltage and remanent polarization exist at voltage amplitudes greater than 10 V and small ion formation energies $\Delta G_i^{00} \leqslant 0.4$ eV.

At equal $\Delta G_1^{00} = \Delta G_2^{00} = 0.5$ eV, the double hysteresis loop occurs indicating the transition to AFI states. The double loops degrade and eventually disappear with increasing value of $\Delta G_1^{00} = \Delta G_2^{00}$ [see plots in Fig. 4 for $\Delta G_1^{00} = \Delta G_2^{00} = 0.9$ eV]. Hence the crossover from the single to double hysteresis loop and then to PE state occurs depending on the ΔG_i^{00} values and their difference.

The physical origin of the double hysteresis loops characteristic to an AFI state in ultrathin films can be explained by the dependence of the surface charge density σ on the electric potential φ given by Eq. (2). The density has the form of a steplike function that is antisymmetric at $\Delta G_1^{00} = \Delta G_2^{00}$ [as shown in Fig. 1(b) by a black curve]. The absolute value of σ is almost zero at an electric potential $\varphi(z = 0)$ lower than $\varphi_i \approx -\Delta G_i^{00}/(eZ_i)$ $(i = 1,2)$, abruptly increases at potential $\varphi = \varphi_i$, and saturates for higher potentials $|\varphi| > |\varphi_i|$. Since the surface charge is responsible for the polarization screening in a ferroelectric film, high charge densities, which correspond to electric potential $|e\varphi| > \Delta G_i^{00}/(eZ_i)$, can provide its almost complete screening, and the low densities, which correspond to potentials $|e\varphi| \leqslant \Delta G_i^{00}/(eZ_i)$, can provide a weak incomplete screening only. Since the potential φ at $z = 0$ is defined by applied voltage U, voltages U_i for which $\varphi(U_i) = \varphi_i$ should exist. Voltages higher that U_i provide a screening degree enough to support the ferroelectric order in a 10-nm film, and so double hysteresis loops of surface charge density and polarization occur.

The above speculations point out that the critical thickness for the film transition from the NFE state to a polydomain or single-domain FE, FI, or AFI states depends on the voltage U. Moreover, the critical thickness decreases with increasing U according to our calculations. Thus an electric field-induced transition to the FI or AFI phases of thin films covered with a layer of ions is possible due to the field stimulation of the electrochemical reaction of ion formation. For instance, the 10-nm film revealed the unusual field-induced transition into FI and AFI states induced by the strong field dependence of the ion charge density. Note that the electric field induced FE state has been observed in ferroelectrics since the 90's [46–48].

At room temperatures, the 10-nm PZT film is in the FI state for $0 \leqslant \Delta G_i^{00} \leqslant 0.1$ eV, and relatively weak ionic screening of its depolarization field is enough to support the state. The corresponding hysteresis loop has a single ferroelectriclike shape with relatively high remanent polarization and coercive voltage. The polarization behavior changes drastically with increasing ΔG_i^{00} when the film approaches the AFI or NFE states. A high screening degree leads to higher critical thickness of the transition [1,15]. Thus additional screening by ions is urgently required to maintain the thin film in a polarized or antipolarized state. The situation for thicker films (e.g., 25-nm thick and more) appeared more usual, since the single loop opens at high voltages for all ΔG_i^{00}, and its width and asymmetry depends much less on ΔG_i^{00} values (see Fig. S3 in Ref. [38]).

A detailed comparison of Figs. 4(a) and 4(b) brings forth the question, how to explain the strong decrease (up to the absence)

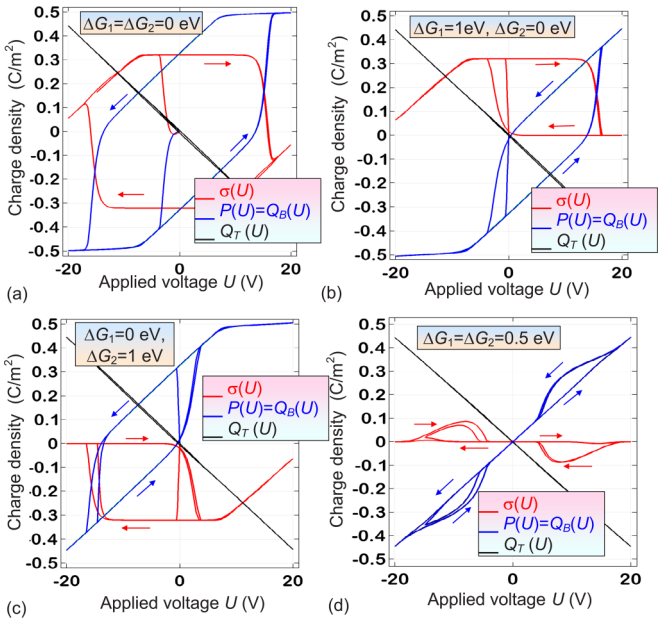

FIG. 5. Dependencies of average polarization $P(U)$ and surface charge $\sigma(U)$ on applied voltage U calculated for a 10-nm PZT film with fixed values $\{\Delta G_1^{00}, \Delta G_2^{00}\}$ indicated in the labels at plots (a)–(d). Arrows indicate the direction of the loops path-tracing; $T = 300$ K, the other parameters are the same as in Fig. 2.

of the surface charge at high voltages [(10–20)V] if the polarization saturates at the same time [e.g., compare the plots of $P(U)$ and $\sigma(U)$ calculated for $\{\Delta G_1^{00}, \Delta G_2^{00}\} = \{0.1, 0.1\}$]? To disclose the reason, we calculated the polarization, surface charge, electric potential, and field at the surface of a 10-nm PZT film at room temperature, where the surface ions are located for a wider range of applied voltages (see Figs. S4 in Ref. [38]). It appeared that the potential becomes very small (and hence the ion charge is small), and the potential and field drop is located in the ultrathin physical gap of thickness $\lambda = 0.4$ nm (see Fig. S4(f) in Ref. [38]). On the other hand, the field inside the film is much smaller and displays hysteretic behavior (see Fig. S4(e) in Ref. [38]). Figure S5 (Ref. [38]) is for the same 10-nm PZT film in a deep paraelectric phase (at high temperature).

We have further calculated the voltage dependence of the total charge at bottom ($z = h$) and top ($z = -\lambda$) electrodes, $Q_B(U)$ and $Q_T(U)$, respectively (see Figs. 5). It appeared that the value and hysteresis shape of $Q_B(U)$ almost coincide with the dependence $P(U)$ in the considered quasistatic limit (i.e. at very low frequencies of applied voltage). However, $Q_T(U)$ is linear and so it principally differs from $P(U)$ due to the surface charge hysteresis of $\sigma(U)$, as well as due to the electric field drop in the ultrathin dielectric gap that "conduct" only the displacement currents. Counterclockwise path tracing of $P(U)$ loops correspond to clockwise path-tracing of $\sigma(U)$ loops.

Our conclusive remarks of the section are that Figs. 2 –4 suggest that the boundaries between PD-FE, SD-FE, FI, and AFI states are not sharp, similarly to the difference between ferroelectric and pyroelectric states. However, we can actually separate them based on the thickness evolution of the free energy for the polarization, as will be demonstrated below.

IV. FREE ENERGY OF FERROIONIC SYSTEM

Here, we develop a simplified analytical model to get insight into the behaviors of the FI states analyzed numerically in the previous section. Since the stabilization of a single-domain polarization in ultrathin perovskite films takes place due to the chemical switching (see, e.g., Refs. [22–26]), we can consider the ferroelectric film in the SD-FE, FI, AFI, NFE, or PE states and assume that the polarization distribution $P_3(x,y,z)$ is smooth, i.e., the distribution $P_3(x,y,z)$ does not deviate significantly from the value averaged over film thickness $P \equiv \langle P_3 \rangle$. In this case, the behavior of the average polarization P and surface charge density σ can be described via the coupled nonlinear algebraic equations derived in Refs. [34–36].

Here we consider the stationary case, when $\sigma = \sigma_0$ and also $p_{\rm exc} = p_{\rm atm}$. The expression for the free energy G, whose minimization gives the coupled equations for polarization dynamics, has the form

$$\frac{G[P,\Psi]}{S} = h\left(\frac{\alpha_R}{2}P^2 + \frac{\beta}{4}P^4 + \frac{\gamma}{6}P^6\right) - \Psi P - \varepsilon_0 \varepsilon_{33}^b \frac{\Psi^2}{2h} - \frac{\varepsilon_0 \varepsilon_d}{2}\frac{(\Psi - U)^2}{\lambda} + \int_0^{\Psi} \sigma_0[\phi] d\phi. \tag{3}$$

The thickness and temperature dependent function $\alpha_R = \alpha_T(T_C - T) + \frac{g_{33}}{h}\left(\frac{1}{\Lambda_+} + \frac{1}{\Lambda_-}\right)$ is the coefficient $\alpha(T)$ renormalized by "intrinsic" gradient-correlation size effects (the term $\sim g_{33}/h$). The first term in Eq. (3) is the Landau-Ginzburg polarization energy. The second term, ΨP, represents the energy of polarization P interaction with overpotential Ψ. The terms $\varepsilon_0 \varepsilon_{33}^b \frac{\Psi^2}{2h}$ and $\frac{\varepsilon_0 \varepsilon_d}{2}\frac{(\Psi - U)^2}{\lambda}$ are the energies of electric field in the ferroelectric film, and in the gap, correspondingly. The last term, $\int_0^{\Psi} \sigma_0[\phi] d\phi$, is the surface charge energy. The formal minimization, $\frac{\partial G[P,\Psi]}{\partial P} = 0$ and $\frac{\partial G[P,\Psi]}{\partial \Psi} = 0$, couples the polarization and overpotential as follows:

$$\alpha_R P + \beta P^3 + \gamma P^5 = \frac{\Psi}{h} \tag{4a}$$

and

$$\Psi = \frac{\lambda(\sigma - P) + \varepsilon_0 \varepsilon_d U}{\varepsilon_0\left(\varepsilon_d h + \lambda \varepsilon_{33}^b\right)} h. \tag{4b}$$

The energy given by Eq. (3) has an absolute minimum at high Ψ. According to the Biot's variational principle [49], we can further use the incomplete thermodynamic potential, the partial minimization of which over P will give the coupled equations of state, and, at the same time, it has an absolute minimum at finite P values. In Appendix B, we derived the P-dependent thermodynamic potential $F[P]$. Assuming that $|eZ_i\Psi/k_BT| \ll 1$, the series expansion of $F[P]$ on polarization powers has the form

$$F \approx A_R \frac{P^2}{2} + B_R \frac{P^4}{4} + C_R \frac{P^6}{6} - P E_{\rm eff}. \tag{5a}$$

Here, the renormalized coefficients are

$$A_R = \frac{\lambda}{\varepsilon_0\left(\varepsilon_d h + \lambda\varepsilon_{33}^b\right)} + f\left(\Delta G_i^{00},h,T\right)\alpha_R(T), \quad (5b)$$

$$B_R = \beta f\left(\Delta G_i^{00},h,T\right),\ C_R = \gamma f\left(\Delta G_i^{00},h,T\right), \quad (5c)$$

The function f in Eqs. (5b) and (5c) is

$$f\left(\Delta G_i^{00},h,T\right) = 1 + \frac{\lambda h}{\varepsilon_0\left(\varepsilon_d h + \lambda\varepsilon_{33}^b\right)} \times \sum_{i=1,2}\frac{(eZ_i)^2}{A_i k_B T}\left[1+\exp\left(\frac{\Delta G_i^{00}}{k_B T}\right)\right]^{-2}. \quad (6)$$

Because the renormalized coefficients B_R and C_R are always positive, the potential (5) has a local minimum in the dependence on the A_R sign and the effective field strength. The effective field produced by the ionic charge has the form

$$E_{\text{eff}}\left(U,\Delta G_i^{00}\right) = \frac{\lambda}{\varepsilon_0\left(\varepsilon_d h + \lambda\varepsilon_{33}^b\right)} \times \sum_{i=1,2}\frac{eZ_i}{A_i}\left[1+\exp\left(\frac{\Delta G_i^{00}}{k_B T}\right)\right]^{-1} - \frac{\varepsilon_d U}{\varepsilon_d h + \lambda\varepsilon_{33}^b}, \quad (7)$$

Since usually $\lambda \ll h$, the effective electric field (6) is proportional to $1/h$ and so E_{eff} becomes higher in thinner films. To study the polarization reversal, E_{eff} should be compared with the intrinsic thermodynamic coercive field E_c for the actual range of temperatures and thickness. To determine E_c, we solve the elementary equation of state $A_R P + B_R P^3 + C_R P^5 = E_{\text{eff}}$. The field E_C defined directly from the equation has the form

$$E_C = \frac{2}{5}(2B_R + \sqrt{9{B_R}^2 - 20A_R C_R}) \times \left(\frac{2A_R}{-3B_R - \sqrt{9{B_R}^2 - 20A_R C_R}}\right)^{3/2}. \quad (8)$$

The coercive field $E_C = \frac{2}{3\sqrt{3}}\sqrt{-\frac{{A_R}^3}{B_R}}$ at $C_R = 0$. Because the coefficients A_R, B_R, and C_R are thickness-dependent, the coercive field is thickness-dependent as well.

We further analyze the dependencies of the effective field, free energy, and polarization states on the ion formation energies, temperature, and film thickness. The effective field E_{eff} induced by the surface ions was calculated at $U = 0$ as a function of the surface ion formation energies ΔG_i^{00} for PZT film thickness $h = 10$, 50, and 100 nm, as shown in Fig. 3(d). The contours of constant field delineate the boundary between FI and SD-FE states in 100-nm and 50-nm thick PZT films [see dashed curves in Figs. 3(a) and 3(b)], as well as the field defines the boundary between FI and NFE states in the thin 10-nm film [shown by dashed curves in Fig. 3(c)]. This confirms the conjecture that the fields induced by surface ions can polarize thin ferroelectric films and prevent the domain formation for the films of thickness less than critical.

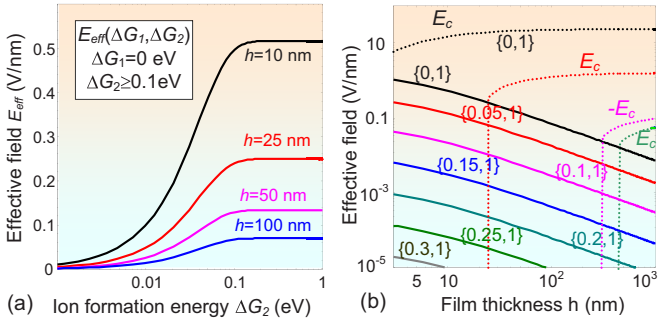

FIG. 6. (a) Effective field $E_{\text{eff}}(\Delta G_1^{00},\Delta G_2^{00})$ depending on the surface ion formation energy ΔG_2^{00} calculated at $\Delta G_1^{00} = 0$. Different curves correspond to PZT film thickness $h = 10$, 25, 50, and 100 nm (as indicated by legends). (b) Thickness dependence of effective field $E_{\text{eff}}(\Delta G_1^{00},\Delta G_2^{00})$ calculated for several pairs of values $\{\Delta G_1^{00},\Delta G_2^{00}\}$ (legends near the curves in eV, where ΔG_1^{00} varies and $\Delta G_2^{00} = 1$ eV). Coercive fields $E_C[h]$ are shown by dashed curves. Temperature $T = 300$ K, $U = 0$, and other parameters are the same as in Fig. 3.

Note that the effective field [see Eq. (7)] is antisymmetric with respect to ΔG, namely $E_{\text{eff}}(0,\Delta G) = -E_{\text{eff}}(\Delta G,0)$. The dependence of $E_{\text{eff}}(\Delta G_1^{00},\Delta G_2^{00})$ versus ΔG_2^{00} was calculated from Eq. (7) for $\Delta G_1^{00} = 0$, $U = 0$ and different thickness $h = (10$–$100)$ nm PZT films [see different curves in Fig. 6(a)]. The field rapidly increases with ΔG_2^{00} increase from 0 to 0.1 eV and then saturates. At that, the saturation value of E_{eff} increases with decreasing film thickness from 0.08 V/nm for 100-nm film to 0.5 V/nm for 10-nm film. The thickness dependence of $E_{\text{eff}}(\Delta G_1^{00},\Delta G_2^{00})$ was calculated for several pairs of $\{\Delta G_1^{00},\Delta G_2^{00}\}$ and compared with the thermodynamic coercive fields $E_C[h]$. The results are shown in Fig. 6(b). It is seen that the coercive field abruptly vanishes with increasing film thickness, and the critical thickness for which this happens depends on the values of $\{\Delta G_1^{00},\Delta G_2^{00}\}$; in particular, it increases with increasing ΔG_1^{00} at fixed $\Delta G_2^{00} = 1$ eV (see also Figs. S6 in Ref. [38]). The effective field exists in ultrathin films, and here it formally dominates over zero coercive fields.

Elementary analysis of the algebraic equation $A_R P + B_R P^3 + C_R P^5 = E_{\text{eff}}$, the mathematical form of which coincides with a conventional Landau equation in external field E_0, shows that the equation has three real roots in the case of the purely second-order phase transitions ($A_R < 0$, $B_R > 0$, $C_R = 0$). One of these roots is absolutely unstable and two others are absolutely stable or metastable depending on the temperature, applied voltage, and film thickness [see global and local minima and maxima in Figs. 7(a) and 7(b) for 100-nm and 50-nm films at room temperature]. In particular, the only real root, $P \approx E_{\text{eff}}/A_R$, exists at $A_R > 0$ for small thicknesses and/or high temperatures [see global minimum in Fig. 7(b) for 10-nm films at room temperature]. The dependence of the absolutely stable polar state P_1 on the surface ion formation energies ΔG_i^{00} calculated for the film thickness $h = 100$, 50, and 10 nm are shown in Figs. 7(c)–7(e), respectively. Notice that the polar states P_i are significantly ΔG_i^{00}-dependent only at $0 \leqslant \Delta G_i^{00} \leqslant 0.1$ eV. Stable, metastable, and unstable polar states in dependence on the surface ions formation energies ΔG_i^{00} were calculated for PZT film thickness $h = 10$, 50, 100, and 300 nm, temperatures 600 and 300 K. The results are shown in Figs. S7–S9.

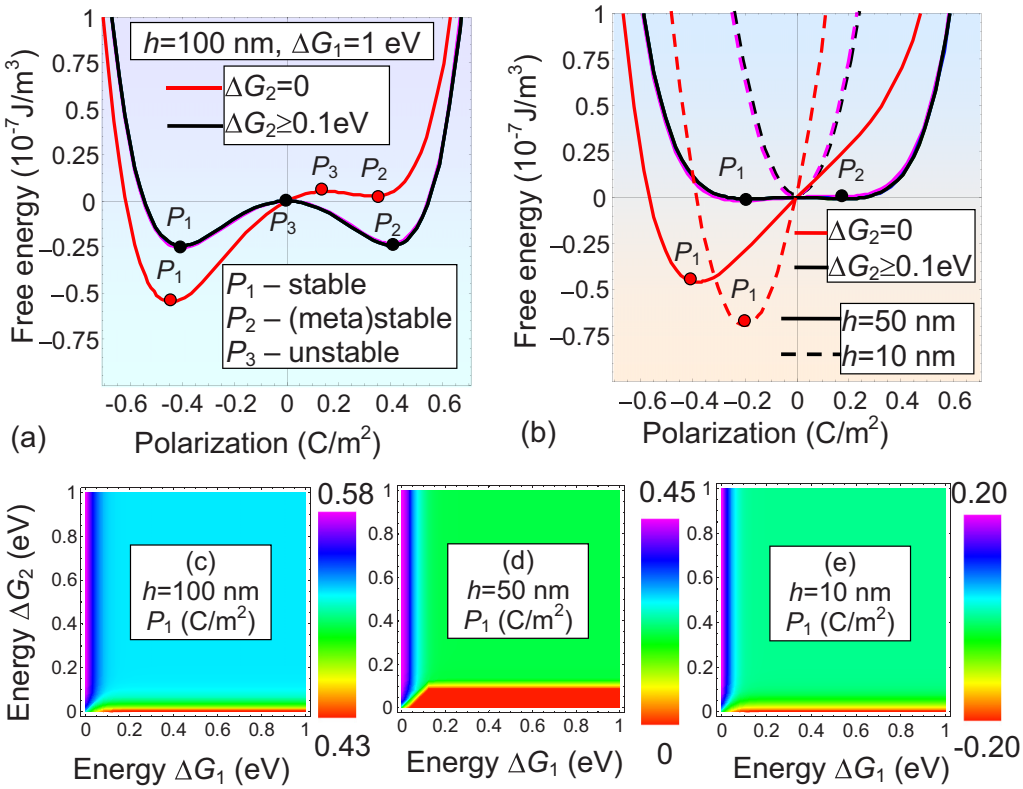

FIG. 7. Dependencies of the free energy on the average polarization calculated in the case of screening by ions, zero applied voltage, and different values of PZT film thickness $h = 100$ (a), 50 (solid curves) and 10 (dashed curves) nm (b). Each curve corresponds to $\Delta G_1^{00} = 1$ eV and $\Delta G_2^{00} = 0$ (red) or $\Delta G_2^{00} = (0.1\text{–}1)$ eV (black an other colors, which coincide). [(c) and (e)] Dependence of the absolutely stable polar state P_1 on the surface ion formation energies ΔG_i^{00} calculated for $h = 100$, 50, and 10 nm (legends at the plots). Color scale bar is polarization in C/m^2; $T = 300$ K, $U = 0$, and other parameters are the same as in Fig. 3.

Because the coefficients A_R, B_R, and C_R depend on the ion formation energies ΔG_i^{00} as per Eq. (5), the free energy (5) is ΔG_i^{00}-dependent, Figs. 8 demonstrate how strong and nontrivial the dependence is for different film thicknesses. For the 300-nm film, there are two deep absolute and local minima, and one high maximum (barrier), whose depth and position are ΔG_2^{00}-dependent at $0 \leqslant \Delta G_2^{00} \leqslant 0.1$ eV and fixed $\Delta G_1^{00} = 1$ eV [Fig. 8(a)]. The minima become much shallower and the barrier almost disappears with the film thickness decrease up to 50 nm [compare the maps in Figs. 8(b) and 8(c)]. Only one absolute minimum exists for the 10-nm film [Fig. 8(d)].

Figure 9 illustrates the dependence of the free energy on the average polarization P and film thickness h calculated for $\Delta G_2^{00} = 0$ [Fig. 9(a)] and $\Delta G_2^{00} = 0.1$ eV [Fig. 9(b)] at fixed $\Delta G_1^{00} = 1$ eV and room temperature. Two nonequivalent minima of polarization (P_1 and P_2) are separated by a barrier (P_3 state) at $\Delta G_2^{00} = 0$ and fixed h above 100 nm, and the only minimum remains for thin films of, e.g., 10-nm thick [see polarization points in Fig. 9(a)]. Two almost equivalent minima of polarization (P_1 and P_2) are separated by a barrier (P_3) at $\Delta G_2^{00} = 0.1$ eV and fixed thickness h more than 50 nm. The minima and barrier transform into a saddle point with decreasing film thickness [see polarization points in Fig. 9(b)]. In fact, Fig. 9 argues that the difference between SD-FE and FI states is not sharp, similarly to the difference between ferroelectric and pyroelectric states, but we can actually separate them based on the thickness evolution of free energy for polarization. For thick films, there are two minima, and they are almost the same as in the bulk. For small thickness, we start to see the mergence of the minima and disappearance of the corresponding polarization state. Thus the ferroionic system undergoes a second-order transition with decreasing film thickness.

The temperature dependencies of three polarization states for a 100-nm film, which correspond to the three roots of algebraic equation $A_R P + B_R P^3 + C_R P^5 = E_{\text{eff}}$ for the case of the second-order phase transitions ($A_R < 0$, $B_R > 0$, $C_R = 0$), are shown by red, magenta, and blue curves, respectively, in Fig. 10(a). Each curve in the group (denoted by single color) corresponds to the definite value of ΔG_2^{00} within the range (0–0.9) eV. The only stable polar state $P \approx E_{\text{eff}}/A_R$ exists in a 10-nm film because $A_R > 0$ for this case [see Fig. 10(b)]. The corresponding dependencies of the polarization states on the surface ion formation energy ΔG_2^{00}.calculated for $T = 300$ and 600 K are shown in Figs. 10(c) and 10(d).

V. DISCUSSION AND OUTLOOK

We established the role of the surface ion formation energies on the polarization states and its reversal scenarios, domain structure, and corresponding phase diagrams of ferroelectric

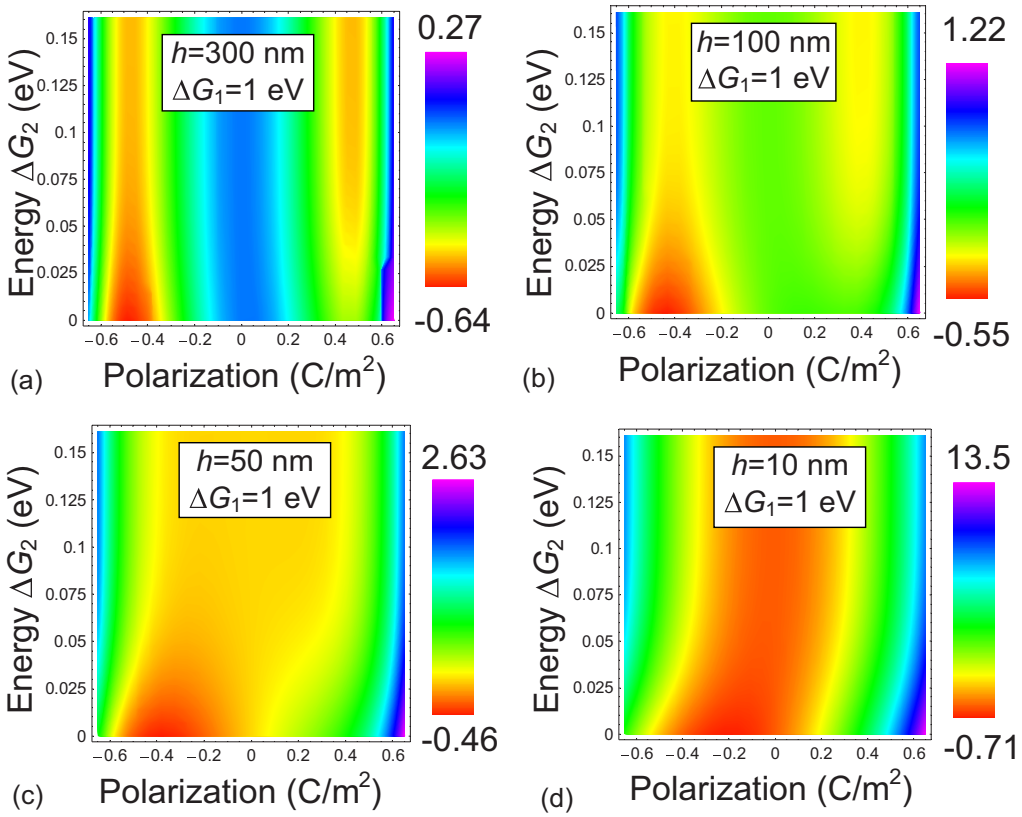

FIG. 8. Dependence of the free energy on the average polarization and surface ion formation energy ΔG_2^{00} calculated for $\Delta G_1^{00} = 1\,\text{eV}$, PZT film thickness $h = 300$ (a), 100 (b), 50 (c), and 10 nm (d). Color scale bar is the energy in $10^7\,\text{J/m}^3$; $T = 300\,\text{K}$, $U = 0$, and other parameters are the same as in Fig. 3.

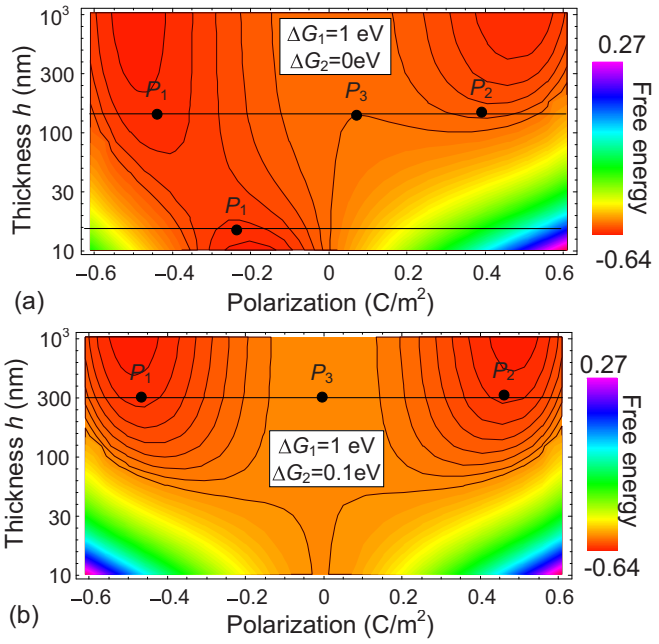

FIG. 9. Dependence of the free energy on the average polarization and PZT film thickness calculated for $\Delta G_1^{00} = 1\,\text{eV}$, $\Delta G_2^{00} = 0$ (a) and $\Delta G_2^{00} = 0.1\,\text{eV}$ (b). Color scale bar is the energy in $10^7\,\text{J/m}^3$; $T = 300\,\text{K}$, $U = 0$, and other parameters are the same as in Fig. 3.

thin films. It appeared that the influence of the physical gaps on the domain formation and stability is very strong. Using 3D finite elements modeling, we analyze the distribution and hysteresis loops of ferroelectric polarization and ionic charge, and the dynamics of the domain states. The obtained results delineate the regions of single- and polydomain ferroelectric, ferroionic, antiferroionic, and nonferroelectric states as a function of surface ions formation energies ΔG_i^{00}, film thickness h, applied voltage U, and temperature T.

We revealed the unusual dependence of the film polar state and domain structure parameters on the ion formation energy value and, what is more unexpected, on the applied voltage. In particular, we observed the voltage-induced phase transition into the single-domain ferroionic states in a thin film covered with an ion layer of electrochemically active nature, when the energies ΔG_i^{00} are significantly different ($|\Delta G_1^{00} - \Delta G_2^{00}| \geqslant 0.2\,\text{eV}$). The voltage-induced phase transition to the antiferroionic state, which is characterized by double hysteresis loops of polarization and surface charge in a wide temperature range, takes places when the energies ΔG_i^{00} are close ($|\Delta G_1^{00} - \Delta G_2^{00}| < 0.05\,\text{eV}$). The physical origin of the double hysteresis loops can be explained by the dependence of the surface charge density on the electric potential, which has the form of the steplike Langmuir absorption isotherm.

We further map the analytical theory for a 1D system onto an effective Landau-Ginzburg free energy and establish the correspondence between the 3D numerical and 1D analytical results at zero applied voltage. The results argue

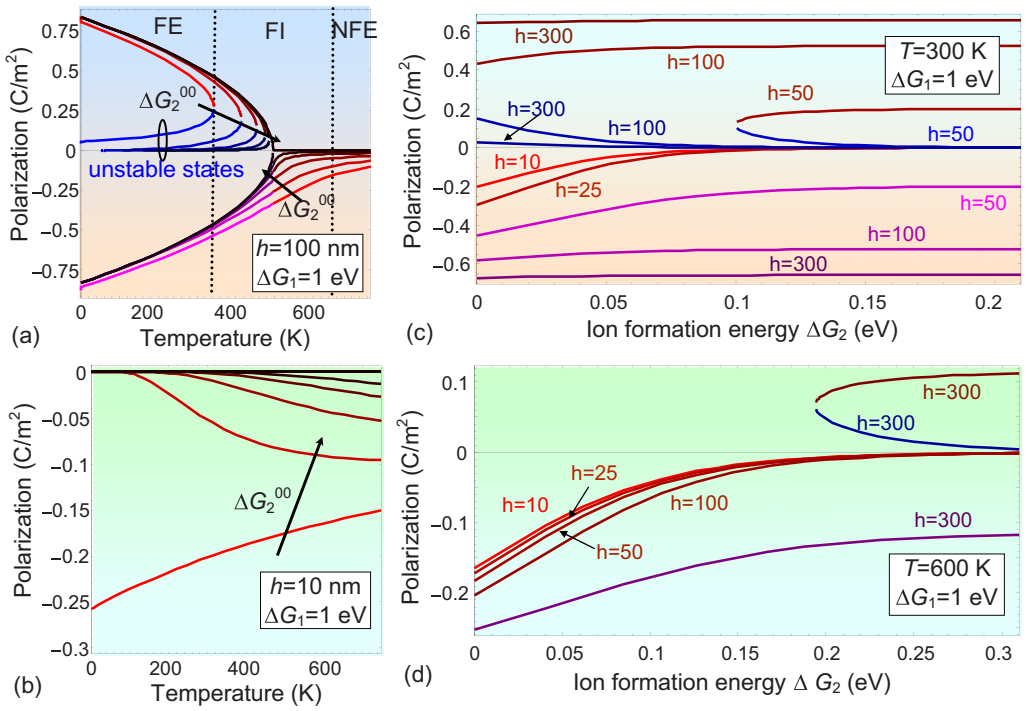

FIG. 10. [(a) and (b)] Temperature dependencies of the average polarization calculated for zero applied voltage and different values of PZT film thickness $h = 100$ (a) and 10 nm (b). Each curve in the one-colored group corresponds to the definite value of $\Delta G_2^{00} = (0,0.05,0.1,0.15,0.2,0.9)$ eV. The arrows indicate the direction of ΔG_2^{00} increase. Unstable branches (inside the ellipse) are shown by blue colors. [(c) and (d)] Dependence of the polarization states on the surface ion formation energy ΔG_2^{00}.calculated for $T = 300$ (c) and 600 K (d). Different curves correspond to $h = 10, 25, 50, 100$, and 300 nm (as indicated by legends in nm). Stable polar states [P_1 and P_2 in Figs. 6(a) and 6(b)] are shown by red and magenta colors. Unstable states [P_3 in Figs. 6(a) and 6(b)] existing for $h \geqslant 50$ nm; they are shown by blue colors. The energy $\Delta G_1^{00} = 1$ eV, $U = 0$, and other parameters are the same as in Fig. 3.

that the difference between the single domain ferroelectric and different ferroionic states is not sharp, similarly to the difference between ferroelectric and pyroelectric states, and we can actually separate them based on the thickness dependence of the ferroionic system free energy. For thick films ($h \geqslant 100$ nm), there are two minima, and the free energy relief is almost the same as in the bulk. For small thickness ($h < 50$ nm), we start to see the mergence of the minima and disappearance of the corresponding polarization state. As a result, the system undergoes the sort of the second-order transition to the ferroionic state taking place with the film thickness decrease.

This approach allows us to get an overview of the ferroionic systems phase diagrams, as well as it reveals the specific features of polarization reversal and domain evolution phenomena. On the other hand, many important questions remain for further studies.

Firstly, if the concentration of the ions becomes smaller, the distance between them increases as its square root. When the distance between the surface ions becomes compatible (or even smaller) with the film thickness, each of the ions should be considered as a point charge defect and the continuous approximation for their charge density $\sigma_0[\varphi]$ becomes invalid. Complementary atomistic calculations should be performed in the case of small ion concentration and/or high saturation densities of the surface ions defining their steric limit (saturation area per one ion).

Secondly, a detailed semiphenomenological and semimicroscopic study of the influence of the surface charge parameters, such as their type (oxygen anions and vacancies versus other charges such as protons, hydroxyls, etc.), enthalpy, and/or formation energies seem to be in order. Notice that the study can reveal the steric limit value and all other properties related with their thermal activation including the net forms of the potential dependence of the occupied cites $\theta_i(\varphi)$, which in principle can be different from the Langmuir isotherm (e.g., Frumkin isothermal function [50]).

Thirdly, the dynamical processes, including the polarization and electromechanical response relaxation and their periodic change (crossover between hysteretic and nonhysteretic behaviors) under a periodic applied voltage are poorly studied. An analysis is impossible without the establishment of the correct hierarchy of different charge species relaxation times.

ACKNOWLEDGMENTS

The publication contains the results of studies conducted by President's of Ukraine grant for competitive projects (grant number F74/25879) of the State Fund for Fundamental Research (A.N.M., E.A.E., A.I.K.). The work was supported by the U.S. Department of Energy, Office of Science, Materials Sciences and Engineering Division (RKV, SVK). A portion of this work was conducted at the Center for Nanophase Materials Sciences, which is a US DOE Office of Science User Facility.

APPENDIX A: ELECTROSTATIC EQUATIONS WITH BOUNDARY CONDITIONS

The quasistatic electric field inside the ferroelectric film is defined via the electric potential φ_f as $E_3 = -\partial\varphi_f/\partial x_3$. The potential φ_f satisfies the electrostatic equations for each medium (gap and ferroelectric film), which acquire the form

$$\Delta\varphi_d = 0 \text{ (inside the gap } -\lambda \leqslant z \leqslant 0), \tag{A1a}$$

$$\left(\varepsilon_{33}^b \frac{\partial^2}{\partial z^2} + \varepsilon_{11}^f \Delta_\perp\right)\varphi_f = \frac{1}{\varepsilon_0}\frac{\partial P_3^f}{\partial z} \text{ (inside the ferroelectric film } 0 < z < h), \tag{A1b}$$

where Δ is the 3D Laplace operator and $\Delta_\perp$ is the 2D Laplace operator. The boundary conditions of the system (A.1) have the form

$$\varphi_d|_{z=-\lambda} = U,\ (\varphi_d - \varphi_f)|_{z=0} = 0,\ \varphi_f|_{z=h} = 0, \tag{A2a}$$

$$\left(\varepsilon_0\varepsilon_d\frac{\partial\varphi_d}{\partial z} + P_3^f - \varepsilon_0\varepsilon_{33}^b\frac{\partial\varphi_f}{\partial z} - \sigma\right)\Big|_{z=0} = 0. \tag{A2b}$$

APPENDIX B: FREE ENERGY WITH RENORMALIZED COEFFICIENTS

If we assume that the polarization distribution $P_3(x,y,z)$ is smooth enough, the coupled nonlinear algebraic equations for the polarization P averaged over the film thickness and surface charge density σ are valid [34–37]:

$$\Gamma\frac{\partial P}{\partial t} + \alpha_R P + \beta P^3 + \gamma P^5 = \frac{\Psi(U,\sigma,P)}{h},\ \tau\frac{\partial\sigma}{\partial t} + \sigma = \sigma_0[\Psi(U,\sigma,P)]. \tag{B1}$$

The overpotential is given by $\Psi(U,\sigma,P) = \frac{\lambda(\sigma-P)+\varepsilon_0\varepsilon_d U}{\varepsilon_0(\varepsilon_d h+\lambda\varepsilon_{33}^b)}h$ and the function $\sigma_0[\psi] = \sum_i \frac{eZ_i\theta_i(\psi)}{A_i} \equiv \sum_i \frac{eZ_i}{A_i}[1+\exp(\frac{\Delta G_i^{00}+eZ_i\psi}{k_BT})]^{-1}$. The electric potentials acting in the dielectric gap (φ_d) and in the ferroelectric film (φ_f) linearly depend on the coordinate z and overpotential, namely $\varphi_d = U - \frac{z+\lambda}{\lambda}(U-\Psi)$ and $\varphi_f = (h-z)\frac{\Psi}{h}$.

Next, we consider the stationary case, when one can put $\sigma = \sigma_0[\Psi(U,\sigma,P)]$ in Eqs. (B1) and (3). The corresponding free energy $G[P,\Psi]$ whose formal minimization, $\frac{\partial G[P,\Psi]}{\partial P} = 0$ and $\frac{\partial G[P,\Psi]}{\partial\Psi} = 0$, leads to Eqs. (B1), has the form

$$\frac{G[P,\Psi]}{S} = h\left(\frac{\alpha_R}{2}P^2 + \frac{\beta}{4}P^4 + \frac{\gamma}{6}P^6\right) - \Psi P - \varepsilon_0\varepsilon_{33}^b\frac{\Psi^2}{2h} - \frac{\varepsilon_0\varepsilon_d}{2}\frac{(\Psi-U)^2}{\lambda} + \int_0^\Psi \sigma_0[\varphi]d\varphi. \tag{B2}$$

The energy (B2) has absolute minima at high Ψ values. So, according to the Biot's variational principle, let us find for the incomplete thermodynamic potential, which partial minimization over P will give the equations of state, and, at the same time, it has an absolute minimum at finite P values. For this purpose, the first of Eqs. (B1) can be considered as an expression for the overpotential dependence on P, i.e., $\Psi[P] = h(\alpha_R P + \beta P^3 + \gamma P^5)$. Substituting here the expression for the overpotential $\frac{\Psi}{h} = \frac{\lambda(\sigma_0[\Psi]-P)+\varepsilon_0\varepsilon_d U}{\varepsilon_0(\varepsilon_d h+\lambda\varepsilon_{33}^b)}$ we derived a single equation for the average polarization:

$$\alpha_R P + \beta P^3 + \gamma P^5 = \frac{\lambda}{\varepsilon_0\left(\varepsilon_d h + \lambda\varepsilon_{33}^b\right)}\sum_{i=1,2}\frac{eZ_i}{A_i}\left\{1+\exp\left[\frac{\Delta G_i^{00} + eZ_i h\left(\alpha_R P + \beta P^3 + \gamma P^5\right)}{k_BT}\right]\right\}^{-1} - \frac{\lambda P - \varepsilon_0\varepsilon_d U}{\varepsilon_0\left(\varepsilon_d h + \lambda\varepsilon_{33}^b\right)}. \tag{B3}$$

The corresponding potential whose minimization over P gives Eq. (B3) has the form

$$F[P] = \left(\begin{array}{l}\left(\frac{\lambda}{\varepsilon_0\left(\varepsilon_d h+\lambda\varepsilon_{33}^b\right)} + \alpha_R\right)\frac{P^2}{2} + \beta\frac{P^4}{4} + \gamma\frac{P^6}{6} + \frac{\varepsilon_d U}{\varepsilon_d h+\lambda\varepsilon_{33}^b}P \\ -\frac{\lambda}{\varepsilon_0\left(\varepsilon_d h+\lambda\varepsilon_{33}^b\right)}\sum\limits_{i=1,2}\frac{eZ_i}{A_i}\int_0^P dp\left[1+\exp\left(\frac{\Delta G_i^{00}+eZ_i h\left(\alpha_R p+\beta p^3+\gamma p^5\right)}{k_BT}\right)\right]^{-1}\end{array}\right). \tag{B4}$$

Assuming that $[1+\exp(\frac{\Delta G_i^{00}+eZ_i\Psi}{k_BT})]^{-1} \approx [1+\exp(\frac{\Delta G_i^{00}}{k_BT})]^{-1}[1 - \frac{eZ_i\Psi}{k_BT(1+\exp(\Delta G_i^{00}/k_BT))}]$ under the condition $|\frac{eZ_i\Psi}{k_BT}| \ll 1$, we derived Eqs. (5)–(7) in the main text.

[1] A. K. Tagantsev, L. E. Cross, and J. Fousek, *Domains in Ferroic Crystals and Thin Films* (Springer, New York, 2010).

[2] A. M. Bratkovsky and A. P. Levanyuk, Continuous theory of ferroelectric states in ultrathin films with real electrodes, J. Comp. Theor. Nanosci. **6**, 465 (2009).

[3] A. M. Bratkovsky and A. P. Levanyuk, Effects of anisotropic elasticity in the problem of domain formation and stability of monodomain state in ferroelectric films, Phys. Rev. B **84**, 045401 (2011).

[4] S. V. Kalinin and D. A. Bonnell, Screening phenomena on oxide surfaces and its implications for local electrostatic and transport measurements, Nano Lett. **4**, 555 (2004).

[5] S. Jesse, A. P. Baddorf, and S. V. Kalinin, Switching spectroscopy piezoresponse force microscopy of

ferroelectric materials, Appl. Phys. Lett. **88**, 062908 (2006).

[6] A. N. Morozovska, S. V. Svechnikov, E. A. Eliseev, S. Jesse, B. J. Rodriguez, and S. V. Kalinin, Piezoresponse force spectroscopy of ferroelectric-semiconductor materials, J. Appl. Phys. **102**, 114108 (2007).

[7] A. V. Ievlev, S. Jesse, A. N. Morozovska, E. Strelcov, E. A. Eliseev, Y. V. Pershin, A. Kumar, V. Y. Shur, and S. V. Kalinin, Intermittency, quasiperiodicity and chaos in probe-induced ferroelectric domain switching, Nat. Phys. **10**, 59 (2013).

[8] A. V. Ievlev, A. N. Morozovska, V. Ya. Shur, and S. V. Kalinin, Humidity effects on tip-induced polarization switching in lithium niobate, Appl. Phys. Lett. **104**, 092908 (2014).

[9] E. V. Chensky and V. V. Tarasenko, Theory of phase transitions to inhomogeneous states in finite ferroelectrics in an external electric field, Sov. Phys. JETP **56**, 618 (1982) [Zh. Eksp. Teor. Fiz. **83**, 1089 (1982)].

[10] P. Ghosez, E. Cockayne, U. V. Waghmare, and K. M. Rabe, Lattice dynamics of BaTiO 3, PbTiO 3, and PbZrO 3: A comparative first-principles study, Phys. Rev. B **60**, 836 (1999).

[11] P. Ghosez and J. Junquera, *First-Principles Modeling of Ferroelectric Oxides Nanostructures* in Handbook of Theoretical and Computational Nanotechnology, edited by M. Rieth and W. Schommers, (American Scientific, Stevenson Ranch, CA, USA, 2006), Chap. 134.

[12] V. R. Aravind, A. N. Morozovska, S. Bhattacharyya, D. Lee, S. Jesse, I. Grinberg, Y. L. Li, S. Choudhury, P. Wu, K. Seal, A. M. Rappe, S. V. Svechnikov, E. A. Eliseev, S. R. Phillpot, L. Q. Chen, V. Gopalan, and S.V. Kalinin, Correlated polarization switching in the proximity of a 180° domain wall, Phys. Rev. B **82**, 024111 (2010).

[13] C.-L. Jia, Knut W. Urban, M. Alexe, D. Hesse, and I. Vrejoiu, Direct observation of continuous electric dipole rotation in flux-closure domains in ferroelectric $Pb(Zr,Ti)O_3$, Science **331**, 1420 (2011).

[14] Y. L. Tang, Y. L. Zhu, X. L. Ma, A. Y. Borisevich, A. N. Morozovska, E. A. Eliseev, W. Y. Wang, Y. J. Wang, Y. B. Xu, Z. D. Zhang, and S. J. Pennycook, Observation of a periodic array of flux-closure quadrants in strained ferroelectric PbTiO3 films, Science **348**, 547 (2015).

[15] I. S. Vorotiahin, E. A. Eliseev, Q. Li, S. V. Kalinin, Y. A. Genenko, and A. N. Morozovska, Tuning the polar states of ferroelectric films via surface charges and flexoelectricity, Acta Materialia **137**, 85 (2017).

[16] E. A. Eliseev, I. S. Vorotiahin, Y. M. Fomichov, M. D. Glinchuk, S. V. Kalinin, Y. A. Genenko, and A. N. Morozovska, Defect driven flexo-chemical coupling in thin ferroelectric films, arXiv:1708.00904.

[17] B. M. Darinskii, A. P. Lazarev, and A. S. Sidorkin, Fiz. Tverd. Tela **31**, 287 (1989) [Sov. Phys. Solid State **31**, 2003 (1989)].

[18] E. A. Eliseev, A. N. Morozovska, S. V. Kalinin, Y. L. Li, Jie Shen, M. D. Glinchuk, L. Q. Chen, and V. Gopalan, Surface effect on domain wall width in ferroelectrics, J. Appl. Phys. **106**, 084102 (2009).

[19] V. Ya. Shur, A. L. Gruverman, V. P. Kuminov, and N. A. Tonkachyova, Dynamics of plane domain walls in lead germanate and gadolinium molybdate, Ferroelectrics **111**, 197 (1990).

[20] E. A. Eliseev, A. N. Morozovska, G. S. Svechnikov, E. L. Rumyantsev, E. I. Shishkin, V. Y. Shur, and S. V. Kalinin, Screening and retardation effects on 180°-domain wall motion in ferroelectrics: Wall velocity and nonlinear dynamics due to polarization-screening charge interaction, Phys. Rev. B **78**, 245409 (2008).

[21] A. I. Kurchak, E. A. Eliseev, S. V. Kalinin, M. V. Strikha, and A. N. Morozovska, P-N junctions dynamics in graphene channel induced by ferroelectric domains motion, Phys. Rev. Appl. **8**, 024027 (2017).

[22] R. V. Wang, D. D. Fong, F. Jiang, M. J. Highland, P. H. Fuoss, C. Thompson, A. M. Kolpak, J. A. Eastman, S. K. Streiffer, A. M. Rappe, and G. B. Stephenson, Reversible Chemical Switching of a Ferroelectric Film, Phys. Rev. Lett. **102**, 047601 (2009).

[23] D. D. Fong, A. M. Kolpak, J. A. Eastman, S. K. Streiffer, P. H. Fuoss, G. B. Stephenson, Carol Thompson, D. M. Kim, K. J. Choi, C. B. Eom, I. Grinberg, and A. M. Rappe, Stabilization of Monodomain Polarization in Ultrathin PbTiO3 Films, Phys. Rev. Lett. **96**, 127601 (2006).

[24] M. J. Highland, T. T. Fister, M.-I. Richard, D. D. Fong, P. H. Fuoss, C. Thompson, J. A. Eastman, S. K. Streiffer, and G. B. Stephenson, Polarization Switching without Domain Formation at the Intrinsic Coercive Field in Ultrathin Ferroelectric PbTiO3, Phys. Rev. Lett. **105**, 167601 (2010).

[25] G. B. StepIehenson and M. J. Highland, Equilibrium and stability of polarization in ultrathin ferroelectric films with ionic surface compensation, Phys. Rev. B **84**, 064107 (2011).

[26] M. J. Highland, T. T. Fister, D. D. Fong, P. H. Fuoss, C. Thompson, J. A. Eastman, S. K. Streiffer, and G. B. Stephenson, Equilibrium Polarization of Ultrathin PbTiO3 with Surface Compensation Controlled by Oxygen Partial Pressure, Phys. Rev. Lett. **107**, 187602 (2011).

[27] Y. Watanabe, Theoretical stability of the polarization in a thin semiconducting ferroelectric, Phys. Rev. B **57**, 789 (1998).

[28] B. M. W. Trapnell, *Chemisorption* (Academic Press, New York, 1955).

[29] T. Wolkenstein, *Electronic Processes on Semiconductor Surfaces during Chemisorption*, translated from Russian by EM Yankovskii and edited by R. Morrison (Consultants Bureau, New York, 1991), p. 35.

[30] V. V. Betsa, V. N. Zhikharev, and Y. V. Popik, Mechanism of adsorption of oxygen and hydrogen on surface of solids, Sov. Phys. J. **20**, 1188 (1977).

[31] Y. V. Popik, V. N. Zhikharev, and V. V. Betsa, Adsorption impact on polarization processes in ferroelectric-semiconductors $BaTiO_3$ and SbSI, Solid State Phys. **24**, 486 (1982).

[32] Y. V. Popik and V. N. Zhikharev, Adsorption impact on polarization value of ferroelectrics, Poverkchnost' (Physics, Chemistry, Mechanics) **6**, 33 (1989).

[33] I. D. Sejkovskij, V. N. Zhiharev, and Yu. V. Popik, Calculation of adsorption and interaction mechanisms of O_2 and CO_2 molecules on $BaTiO_3$ surface, Condens. Matter Phys. **6**, 281 (2003).

[34] S. M. Yang, A. N. Morozovska, R. Kumar, E. A. Eliseev, Y. Cao, L. Mazet, N. Balke, S. Jesse, R. Vasudevan, C. Dubourdieu, and S. V. Kalinin, Mixed electrochemical-ferroelectric states in nanoscale ferroelectrics, Nat. Phys. **13**, 812 (2017).

[35] A. N. Morozovska, E. A. Eliseev, N. V. Morozovsky, and S. V. Kalinin, Ferroionic states in ferroelectric thin films, Phys. Rev. B **95**, 195413 (2017).

[36] A. N. Morozovska, E. A. Eliseev, N. V. Morozovsky, and S. V. Kalinin, Piezoresponse of ferroelectric films in ferroionic states: time and voltage dynamics, Appl. Phys. Lett. **110**, 182907 (2017).

[37] S. V. Kalinin, Y. Kim, D. Fong, and A. Morozovska, Surface screening mechanisms in ferroelectric thin films and its effect on polarization dynamics and domain structures, Rev. Prog. Phys. (to be published).

[38] See Supplementary Materials http://link.aps.org/supplemental/10.1103/PhysRevB.96.245405 for details.

[39] A. K. Tagantsev and G. Gerra, Interface-induced phenomena in polarization response of ferroelectric thin films, J. Appl. Phys. **100**, 051607 (2006).

[40] E. A. Eliseev and A. N. Morozovska, General approach to the description of the size effect in ferroelectric nanosystems, J. Mater. Sci. **44**, 5149 (2009).

[41] R. Kretschmer and K. Binder, Surface effects on phase transitions in ferroelectrics and dipolar magnets, Phys. Rev. B **20**, 1065 (1979).

[42] C.-L. Jia, V. Nagarajan, J.-Q. He, L. Houben, T. Zhao, R. Ramesh, K. Urban, and R. Waser, Unit-cell scale mapping of ferroelectricity and tetragonality in epitaxial ultrathin ferroelectric films. Nat. Mater. **6**, 64 (2007).

[43] K. Y. Foo and B. H. Hameed, Insights into the modeling of adsorption isotherm systems, Chem. Eng. J. **156**, 2 (2010).

[44] A. I. Kurchak, A. N. Morozovska, S. V. Kalinin, and M. V. Strikha, Nontrivial temperature behavior of the carriers concentration in the nano-structure "graphene channel - ferroelectric substrate with domain walls" (unpublished).

[45] Y. Cao and S. V. Kalinin, Phase-field modeling of chemical control of polarization stability and switching dynamics in ferroelectric thin films, Phys. Rev. B **94**, 235444 (2016).

[46] O. E. Fesenko, *Phase Transitions in Ultra-High Electric Fields* (Rostov University Publ., Rostov-on-Don, 1984) (In Russian).

[47] X. Ren, Large electric-field-induced strain in ferroelectric crystals by point-defect-mediated reversible domain switching, Nat. Mater. **3**, 91 (2004).

[48] D. J. Franzbach, Y. J. Gu, L. Q. Chen, and K. G. Webber, Electric field-induced tetragonal to orthorhombic phase transitions in [110]c-oriented BaTiO3 single crystals, Appl. Phys. Lett. **101**, 232904 (2012).

[49] B. D. Vujanovic, and S. E. Jones, *Variational Methods in Nonconservative Phenomena* (Academic Press, San Diego, 1989).

[50] A. N. Frumkin, O. A. Petrii, and B. B. Damaskin, *Potentials of zero charge* in Comprehensive Ttreatise of Electrochemistry, edited by J. O'M. Bockris, B. E. Conway, and E. B. Yeager (Plenum, New York, 1980), Vol. 1, pp. 221–289.